Published in final edited form as:
J Cell Sci. 2008 June 1; 121(Pt 11): 1907–1915. doi:10.1242/jcs.029397.

The intraflagellar transport protein IFT57 is required for cilia maintenance and regulates IFT-particle–kinesin-II dissociation in vertebrate photoreceptors

Bryan L. Krock and **Brian D. Perkins***
Department of Biology, Texas A&M University, College Station, TX 77843, USA

Abstract

Summary—Defects in protein transport within vertebrate photoreceptors can result in photoreceptor degeneration. In developing and mature photoreceptors, proteins targeted to the outer segment are transported through the connecting cilium via the process of intraflagellar transport (IFT). In studies of vertebrate IFT, mutations in any component of the IFT particle typically abolish ciliogenesis, suggesting that IFT proteins are equally required for IFT. To determine whether photoreceptor outer segment formation depends equally on individual IFT proteins, we compared the retinal phenotypes of IFT57 and IFT88 mutant zebrafish. IFT88 mutants failed to form outer segments, whereas IFT57 mutants formed short outer segments with reduced amounts of opsin. Our phenotypic analysis revealed that IFT57 is not essential for IFT, but is required for efficient IFT. In co-immunoprecipitation experiments from whole-animal extracts, we determined that kinesin II remained associated with the IFT particle in the absence of IFT57, but IFT20 did not. Additionally, kinesin II did not exhibit ATP-dependent dissociation from the IFT particle in IFT57 mutants. We conclude that IFT20 requires IFT57 to associate with the IFT particle and that IFT57 and/or IFT20 mediate kinesin II dissociation.

Keywords

Retinal degeneration; Opsin trafficking; Zebrafish

Introduction

Vertebrate photoreceptors are highly specialized neurons that possess a modified sensory cilium known as the outer segment. The outer segment develops as an extension of a nonmotile primary cilium (De Robertis, 1960). As the outer segment lacks the machinery for protein synthesis, all protein destined for the outer segment must pass through the connecting cilium. Large amounts of protein synthesized in the inner segment must be efficiently transported to the outer segment to replenish material lost from the distal tips each day. Estimates from mammalian systems have calculated ~2000 rhodopsin molecules per minute must be transported to the outer segment to compensate for lost material (Besharse, 1990). Hence, both the development and survival of the photoreceptor require this continual transport of protein to the outer segment (Marszalek et al., 2000).

Studies of rhodopsin trafficking in several species have linked defects in protein transport to photoreceptor degeneration and the disease retinitis pigmentosa. The C-terminal tail of

*Author for correspondence (e-mail: bperkins@mail.bio.tamu.edu)

Supplementary material available online at http://jcs.biologists.org/cgi/content/full/121/11/1907/DC1

rhodopsin contains a sorting sequence that is necessary and sufficient for transport to the outer segment (Perkins et al., 2002; Tam et al., 2000). Mutations in this region result in protein accumulation in the inner segment and at the base of the connecting cilium in mice, rats and frogs (Green et al., 2000; Li et al., 1996; Sung et al., 1994; Tam et al., 2000), leading to photoreceptor degeneration. Indeed, mutations in the C terminus of human rhodopsin, such as P347L and S344Ter, can cause retinitis pigmentosa (Berson et al., 1991). Rhodopsin mislocalization also occurs in animals with mutations in the molecular motors kinesin II (Marszalek et al., 2000) and the dynein light chain Tctex-1 (Tai et al., 1999), both of which show severe retinal degeneration. It is imperative, therefore, that cargo targeted for the outer segment reach its destination or retinal degeneration will occur. Thus, both mutations within the opsin gene and mutations in the transport machinery can cause retinal degenerative diseases.

Protein transport along a ciliary axoneme, such as the connecting cilium, occurs via the process known as intraflagellar transport (IFT) (Rosenbaum and Witman, 2002). Both the assembly and maintenance of cilia require IFT and defects in ciliogenesis have been linked to retinal degeneration, polycystic kidney disease, Bardet-Biedl syndrome, Jeune asphyxiating thoracic dystrophy, respiratory disease and defective left-right axis determination (Beales et al., 2007; Pazour and Rosenbaum, 2002; Snell et al., 2004). IFT refers to movement of the IFT particle, a multisubunit protein complex that consists of at least 17 IFT proteins that form two subcomplexes: complex A and complex B (Cole et al., 1998). The IFT particle associates with heterotrimeric kinesin II, which comprises two motor subunits and an accessory subunit, known as KIF3A, KIF3B and KAP, respectively (reviewed by Cole, 1999). Kinesin II cooperates with a homodimeric kinesin known as OSM-3 to mediate transport of the IFT particle and its associated cargo toward the ciliary tip (Cole et al., 1998; Orozco et al., 1999; Ou et al., 2005; Snow et al., 2004). The process of IFT is highly conserved, as mutations in IFT proteins perturb ciliary assembly and/or maintenance in organisms as diverse as *Chlamydomonas*, *C. elegans*, *Drosophila*, mouse, humans and zebrafish (Beales et al., 2007; Cole et al., 1998; Han et al., 2003; Murcia et al., 2000; Pazour et al., 2000; Pedersen et al., 2005; Sun et al., 2004; Tsujikawa and Malicki, 2004).

Recent biochemical studies, predominantly in *Chlamydomonas*, have started to reveal the structural composition of the IFT particle and specific interactions between individual IFT proteins, particularly within complex B. Eleven proteins constitute the *Chlamydomonas* complex B, a subset of these forms a core consisting of an IFT72/74-IFT80 tetramer along with IFT88, IFT81, IFT52 and IFT46 (Lucker et al., 2005). The outer surface of complex B is composed of IFT20, IFT57, IFT80 and IFT172. Data from yeast two-hybrid experiments indicate direct interactions between IFT72/74 and IFT81, and between IFT57 and IFT20. Similar approaches have indicated interactions between IFT20 and the KIF3B subunit of kinesin II (Baker et al., 2003; Lucker et al., 2005). Although the IFT72/74-IFT80 interaction probably forms the structural core of complex B, the functional nature of the interactions described for the outer surface IFT proteins remains unclear.

Previous studies investigating mutations in IFT genes have revealed few phenotypic differences in ciliated structures of any tissue. In *Chlamydomonas*, mutations in genes coding for complex B proteins, such as IFT52, IFT88 and IFT172, result in a complete absence of flagella (Cole, 2003). IFT88 mutations have been shown to abolish cilia in the sensory neurons of *C. elegans* and *Drosophila* (Han et al., 2003; Haycraft et al., 2001). In zebrafish, mutants of IFT88 and IFT172 lack outer segments entirely, and IFT88 mutants lack all sensory cilia at 4 days post fertilization (dpf) (Gross et al., 2005; Tsujikawa and Malicki, 2004). In mice, all null alleles of IFT88 and IFT172 cause embryonic lethality before E12, thereby preventing analysis of photoreceptor structure, though nodal cilia are completely absent in these animals (Huangfu et al., 2003; Murcia et al., 2000). In $Tg737^{orpk}$ mutants, which have a hypomorphic mutation in murine IFT88, photoreceptors display aberrant outer segment disk stacking,

accumulation of vesicles and progressive photoreceptor degeneration (Pazour et al., 2002; Pazour et al., 2000). However, recent evidence suggests that loss of individual IFT proteins may not completely abolish ciliogenesis. Although not completely normal, cilia do remain in *Chlamydomonas* cells that lack IFT27, which plays a role in cell cycle regulation (Qin et al., 2007), or IFT46, which facilitates transport of outer dynein arms (Hou et al., 2007). Phenotypic differences have not yet been described in other tissues or species.

Although the photoreceptor phenotypes associated with the partial or complete loss of function of IFT88 have been well characterized in both mouse and zebrafish, no such analysis has been made for most of the remaining 16 or so IFT peptides. Loss-of-function studies with the zebrafish IFT140 and IFT81 did not reveal a retinal phenotype, although the IFT81 mutation did cause cystic kidneys (Gross et al., 2005; Sun et al., 2004; Tsujikawa and Malicki, 2004). Morpholino knockdown of the zebrafish IFT52 and IFT57 genes resulted in a loss of photoreceptors (Tsujikawa and Malicki, 2004); however, the ultrastructure, development and morphology of photoreceptors in these animals were not analyzed. Although photoreceptors clearly require the IFT process for proper outer segment biogenesis, the composition of the IFT particle functioning in the photoreceptor may be different from the one in *Chlamydomonas*. Many cargo molecules destined for the outer segments, such as rhodopsin, are unique to photoreceptors. Vertebrate photoreceptors also have a simpler axonemal structure (9+0 microtubule arrangement) than the one found in the *Chlamydomonas* flagellum or vertebrate motile cilia (9+2 arrangement).

Herein, we analyze zebrafish with an insertional mutation in the *ift57* gene, which have a photoreceptor phenotype that is distinct from IFT88 mutant zebrafish. Our data show that the process of IFT can occur, albeit inefficiently, in the absence of IFT57. Our data also attribute specific functions to IFT57 and IFT20 within the IFT complex, and provide novel insights into how kinesin II dissociates from the IFT particle. This work has implications for both the molecular mechanism of IFT and the molecular requirements for photoreceptor outer segment formation.

Results

To determine the effects different IFT mutations on photoreceptor development, we examined the phenotypes of zebrafish IFT57 and IFT88 mutants. In a screen for photoreceptor defects, we previously identified a mutation in the zebrafish IFT57 homolog (Gross et al., 2005). The hi3417 allele is a retroviral insertional mutation (Amsterdam and Hopkins, 1999) in the first exon of the IFT57 gene. This mutant has been reported to form kidney cysts (Sun et al., 2004), but the retinal phenotype of IFT57 mutants has yet to be fully characterized. Zebrafish *oval* mutants carry an ENU-induced point mutation in the IFT88 gene that introduces a premature stop codon, thereby eliminating function (Tsujikawa and Malicki, 2004).

At 4 days post-fertilization, both IFT57 and IFT88 mutants exhibited a ventral body curvature, had slightly smaller eyes and developed kidney cysts (supplementary material Fig. S1). To confirm that the retroviral insertion in IFT57 causes the observed phenotype, we injected splice site-directed morpholino oligonucleotides into wild-type embryos. Injection of gene-specific morpholinos phenocopied the morphological and kidney phenotypes of both IFT57 and IFT88 mutants (supplementary material Fig. S1). These results show that the general phenotype of both mutants is highly similar, and suggest that the IFT57 mutation represents a functional null allele.

To compare the retinal anatomy of IFT57 and IFT88 mutants, we analyzed histological sections of 4 dpf animals by light microscopy. Retinal lamination and normal cellular differentiation was unaffected in IFT57 and IFT88 mutants at 4 dpf (Fig. 1A-C). Both IFT57 and IFT88

mutants exhibited holes within the photoreceptor layer, which is indicative of cell death, whereas other cell types within the retina were unaffected. Cell death specifically within the outer nuclear layer indicated that photoreceptors are the only cell type within the retina whose survival was affected by the loss of IFT proteins. Consistent with previous findings (Doerre and Malicki, 2002; Tsujikawa and Malicki, 2004), higher magnification images (Fig. 1D-F) found no photoreceptor outer segments in IFT88 mutants. By contrast, IFT57 mutant photoreceptors retained short outer segments in both the periphery and central regions of the retina. Morpholino-injected animals (morphants) were phenotypically identical to the mutants at 4 dpf (Fig. 1E,F, compare with Fig. 1H,I). To test whether the IFT57 mutant phenotype reflected a hypomorphic mutation, we performed western blots on lysates of 4 dpf IFT57 mutant embryos with a polyclonal antibody against the C terminus of zebrafish IFT57 (see Materials and Methods). We did not detect any IFT57 protein in mutant lysates (Fig. 1G), and concluded that the hi3417 allele caused a null mutation in the IFT57 gene. These results demonstrate phenotypic differences resulting from mutations in two different IFT complex B proteins.

As IFT57 mutants produced outer segments, we hypothesized that components of the phototransduction cascade would be transported to the outer segments. Immunohistochemical analysis with an antibody against rhodopsin, 1D1, and an antibody against blue cone opsin revealed both rhodopsin and blue cone opsin were present within the outer segments of IFT57 mutant rods and blue cones, respectively (Fig. 2A-F). Opsin mislocalized to the inner segment in IFT57 mutant photoreceptors, although transport to the outer segments did occur (Fig. 2B,E). Both rhodopsin and blue opsin were completely mislocalized throughout the plasma membrane of IFT88 mutant photoreceptors (Fig. 2C,F). These data indicate that transport to the outer segment via IFT was disrupted but not abolished in the absence of IFT57 but did not occur in the absence of IFT88. To address the issue of whether IFT57 mutants generated connecting cilia, we stained retinal sections with anti-acetylated tubulin (Fig. 2J-L). Consistent with the observation that outer segment formation and opsin transport occurs in IFT57 mutants, we found cilia projecting apically from the inner segment of wild type and IFT57 mutants. Ciliary projections were not observed in IFT88 mutants. However, when stained with ZPR1, a marker for red-green double cone morphology, we found that IFT57 and IFT88 mutant photoreceptor morphology was abnormal (Fig. 2G-I).

As mislocalization of opsin can cause photoreceptor degeneration, and defects in opsin transport are associated with disorganized outer segments (Pazour et al., 2002), we used transmission electron microscopy (TEM) to examine the photoreceptor morphology of 4 dpf IFT57 and IFT88 mutants (Fig. 3A-C). Wild-type photoreceptors had elongated outer segments, while IFT88 mutants exhibited no photoreceptor outer segments. By contrast, both rod and cone outer segments were seen in IFT57 mutants. Consistent with results from immunohistochemistry, basal bodies and connecting cilia were observed in IFT57 mutant photoreceptors. We observed vesicle membranes accumulating near the connecting cilium in IFT57 mutants. These vesicles were similar to those seen in photoreceptors expressing a dominant-negative Rab8, which disrupted transport of vesicular cargo through the connecting cilium (Moritz et al., 2001). These membranes were probably post-Golgi vesicles that reflect inefficient protein transport through the outer segment, which is consistent with results of opsin mislocalization in the inner segment. Although the outer segments were shorter and ciliary transport was affected, the disk membranes remained well ordered and tightly stacked in the IFT57 mutants. Upon quantification, IFT57 mutants were found to have photoreceptor outer segments that were reduced in length by 75% compared with wild-type photoreceptors (Fig. 4A).

To quantify how the loss of IFT57 and IFT88 affected rhodopsin transport, we performed immunogold analysis on IFT57 and IFT88 mutants using the anti-rhodopsin antibody 1D1

(Fig. 3F-H). Although the rhodopsin immunogold label localized primarily to the rod outer segments in IFT57 mutants (Fig. 3G), gold particle density was reduced by 59% when compared with age-matched wild-type controls (Fig. 4B). In IFT88 mutants, gold-labeled rhodopsin localized predominantly to the apical part of the inner segment but was also distributed in the plasma membrane (Fig. 3H), indicating that vesicular trafficking from the Golgi to the apical surface is unaffected by loss of IFT88. These data demonstrate that outer segment formation and opsin transport requires IFT88, whereas IFT can function at reduced efficiency without IFT57.

Biochemical studies have shown that IFT57 directly interacts with IFT20 and that IFT20 directly interacts with the KIF3B subunit of kinesin II (Baker et al., 2003). Baker and colleagues (Baker et al., 2003) proposed a model wherein IFT57 recruits IFT20 to the IFT particle and IFT20 serves as the link between kinesin II and the IFT particle. To investigate the nature of the IFT57-IFT20 interaction in vivo, we analyzed the localization of IFT20 in IFT57 mutant photoreceptors. In immunohistochemical analysis, the polyclonal antibodies we generated against IFT20 failed to label with sufficient specificity for conclusive results. We therefore injected one-cell embryos with a plasmid containing an IFT20-GFP fusion protein under the control of a *Xenopus laevis* rhodopsin promoter to express IFT20-GFP transiently in a subset of zebrafish rod photoreceptors. In transgenic rods of 4 dpf wild-type embryos, IFT20-GFP was observed at the base of the connecting cilium, as demonstrated by colocalization with anti-acetylated tubulin (Fig. 5A). IFT20-GFP also localized to the base of the cilium in IFT57 mutant rods, indicating that ciliary localization of IFT20 does not require IFT57 (Fig. 5B). Consistent with recent reports that IFT20 also localized to the Golgi apparatus (Follit et al., 2006), we observed that IFT20-GFP fluorescence colocalized with antibodies against syntaxin 6, a marker for the trans-Golgi network, in both wild type and IFT57 mutants (Fig. 5C,D). As mutation of IFT88 completely abolishes IFT and our IFT57 mutant exhibits some functional IFT, we predicted that loss of IFT57 would not affect the localization of IFT88 to the connecting cilium. When we immunolabeled IFT57 mutant retinal sections with an anti-IFT88 antibody, we observed IFT88 staining that colocalized with acetylated tubulin. The pattern of localization of IFT88 also indicated that IFT88 was present within the connecting cilium itself, consistent with our assertion that IFT57 mutants retain some functional IFT. Taken together, these results indicate that IFT57 is not required for the normal localization of IFT20 or IFT88 to the base of the connecting cilium.

We next analyzed the composition of the IFT particle in IFT57 mutants in order to understand how the process of IFT could occur in the absence of the IFT57 protein. We first performed western blotting experiments on wild-type and IFT57 mutant larval lysates (Fig. 6A). Protein blots probed with antibodies against KIF3A, IFT88, IFT52 and IFT20 showed that IFT protein levels were present at levels that would probably be sufficient for biological activity. As shown previously, we did not detect measurable levels of IFT57 protein in mutant lysates. These results suggested that loss of IFT57 did not significantly alter the expression of other IFT components.

We next performed co-immunoprecipitation experiments on 4 dpf wild-type and IFT57 mutant lysates. Briefly, 4 dpf zebrafish larvae were homogenized and IFT proteins co-immunoprecipitated using a polyclonal antibody against zebrafish IFT88 (Fig. 6B). We found that IFT52, IFT20 and the KIF3A subunit of kinesin II could be co-precipitated from wild-type zebrafish lysates. When these experiments were performed on IFT57 mutant lysates, we found that KIF3A and IFT52 co-precipitated, but IFT20 did not. We were surprised to find that KIF3A co-precipitated from IFT57 mutant lysates, indicating that kinesin II can interact with the IFT particle independent of IFT20.

When we performed the co-immunoprecipitation experiments on IFT57 mutant lysates, we noticed that significantly more KIF3A was present in our precipitates from IFT57 mutant lysates than from wild-type lysates. Given that the process of IFT is defective in IFT57 mutants, but still occurs, we hypothesized that kinesin fails to dissociate from the IFT particle in the absence of IFT57. The interaction between kinesin II and the IFT particle is salt sensitive and ATP dependent, such that addition of 1 mM ATP to lysates blocks precipitation of kinesin II with the IFT particle (Baker et al., 2003). Consistent with these results, we found that kinesin II did not co-precipitate from wild-type lysates in the presence of 1 mM ATP (Fig. 6C). When IFT57 mutant lysates were incubated with 1 mM ATP, however, the association between kinesin II and the IFT particle is maintained (Fig. 6C). However, if protein lysates were incubated with 10 mM ATP, the association between kinesin II and the IFT particle is lost in both wild type and IFT57 mutants (Fig. 6D). These data show that the ATP-dependent dissociation of kinesin II from the IFT particle is impaired, and suggest a role for IFT57 and IFT20 in mediating motor dissociation from the IFT particle.

Discussion

In this study, we investigated and compared the roles of IFT57 and IFT88 in vertebrate photoreceptor development. Unlike the mouse Tg737^{orpk} allele of IFT88, which forms outer segments, the zebrafish IFT57 mutant phenotype is not the result of a hypomorphic allele. Although a genome duplication occurred during the evolution of the lineage leading to zebrafish, only about 30% of these genes were retained (Postlethwait et al., 2000). IFT57 paralogs have not been identified in the zebrafish genome databases that might compensate for its function and generate a hypomorphic phenotype (Sun et al., 2004) (this study). Our western blotting analysis of IFT57 mutants also excludes maternal contribution of protein or mRNA as an explanation for the ciliary phenotype of IFT57 mutants at 4 dpf. Even if an undetectable amount of IFT57 protein exists in IFT57 mutants, the stoichiometric composition of the IFT particle would be perturbed, probably resulting in a null phenotype. Taken together, these results demonstrate that the loss of IFT57 and IFT88 can produce distinct phenotypes that reflect functional roles for these proteins within the IFT complex, as discussed below.

Many studies of loss-of-function phenotypes in vertebrate IFT genes focus attention on phenotypic similarities and rarely emphasize differences, which implies that all IFT mutant phenotypes should be identical. Mutations in the mouse IFT52, IFT57, IFT88 and IFT172 orthologs all lead to identical defects in cilia formation, sonic hedgehog signaling and motoneuron differentiation (Houde et al., 2006; Huangfu et al., 2003; Liu et al., 2005). A mouse knockout of IFT57 was reported to have loss of nodal cilia; however, the analysis did not exclude the possibility of cilia formation and subsequent degeneration (Houde et al., 2006). Morpholinos that disrupt zebrafish IFT88 and IFT57 gene expression produce similar defects in left-right asymmetry, kidney function and cilia motility, although subtle differences in cilia length and phenotypic outcomes were mentioned but not elaborated (Bisgrove et al., 2005; Kramer-Zucker et al., 2005). In zebrafish, a retroviral insertion mutation in the complex B gene IFT81 did not affect photoreceptor development (Gross et al., 2005) but did cause kidney cysts (Sun et al., 2004), whereas morpholino knockdown of a complex A protein, IFT140, did not affect photoreceptor survival (Tsujikawa and Malicki, 2004). Our results provide the first in vivo comparative study of photoreceptor structure and function in two null IFT mutants, and demonstrate that mutations in IFT57 and IFT88 affect different aspects of photoreceptor development.

Our data also indicate that ciliary transport and outer segment morphogenesis requires IFT88, whereas IFT57 is required for effective transport and outer segment maintenance. Transport is also eliminated in IFT88 mutants of *Chlamydomonas*, mice and worms (Haycraft et al., 2001; Pazour et al., 2000; Qin et al., 2001). By contrast, the presence of connecting cilia and

opsin labeling of outer segment structures indicate ciliary transport does occur in IFT57 mutants. It is important to note, however, that transport remains compromised in IFT57 mutants, as indicated by opsin mislocalization to the inner segment, vesicle accumulation at the base of the cilium and an overall reduction in outer segment length.

A previous analysis of a mutation in *CHE-13*, the *C. elegans* ortholog of IFT57, noted that the *CHE-13* phenotype was identical to that of a previously characterized IFT88 mutation (Haycraft et al., 2003). Our analysis, however, indicates that mutation of these two genes results in different outcomes. This may be due to inherent differences in the mechanism of IFT between these two systems. In addition, the authors did not exclude the possibility of formation of these structures and subsequent degeneration, which is what we observed in our study.

Although transport is compromised, disk stacking in IFT57 mutant outer segments was unaffected. Opsin is believed to play an important role in the formation and stabilization of disk membranes within the outer segment (Nathans, 1992). Studies of rhodopsin heterozygous knockout mice found that reducing opsin by ~50% causes disorganization of outer segments and disk stacking, with some abnormally oriented membranes and a complete loss of outer segments in homozygous rhodopsin knockout mice (Humphries et al., 1997; Lem et al., 1999). Rhodopsin levels were reduced by almost 60% in IFT57 mutant photoreceptors, yet no such disorganization of the outer segment was observed. One explanation is that opsin mislocalization kills the photoreceptor before outer segment disorganization occurs. Alternatively, zebrafish outer segments may require less opsin for disk membrane organization and outer segment integrity than do mammalian systems.

Our phenotypic and biochemical analyses of IFT57 support a model for protein interactions within the IFT particle that facilitate ciliary transport and anterograde motor dissociation. We show that IFT20 does not bind the IFT particle in the absence of IFT57, indicating that IFT57 mediates the interaction between IFT20 and the particle. Additionally, kinesin II co-precipitates with the IFT particle in IFT57 mutant lysates. These results indicate that the previously described IFT20-kinesin II interaction (Baker et al., 2003) is not the primary link between kinesin II with the IFT particle. We suggest that kinesin II binds to the IFT particle through an interaction with an unidentified IFT protein. Finally, we have shown that the ATP-dependent dissociation of kinesin II from the IFT particle is inhibited by loss of IFT57. Consistent with this, we also observe a greater quantity of KIF3A in IFT57 mutant precipitates than in wild type precipitates. It is important to note, however, that kinesin II has the ability to dissociate from the IFT particle in IFT57 mutants, as addition of super-physiological levels of ATP (10 mM) can cause dissociation of kinesin II.

We propose that IFT57 mediates the interaction between IFT20 and the IFT particle, whereas an undefined IFT protein or adaptor protein serves as the primary bridge between kinesin II and the IFT particle (Fig. 7). Our data indicates this bridge must be independent of both IFT57 and IFT20. Additionally, we propose that IFT57 and/or IFT20 mediates dissociation of heterotrimeric kinesin II from the IFT particle, potentially by enhancing the ATPase activity of KIF3B. As IFT20 is the only IFT protein known to interact with kinesin II, loss of IFT20 from the IFT particle is the likely explanation for the observed kinesin II dissociation defect. However, we cannot rule out a direct role for IFT57 in this process, though yeast 2-hybrid analysis showed no interaction between IFT57 and any of the kinesin II subunits (Baker et al., 2003). Others have shown that the ATP-mediated dissociation of kinesin II from the IFT particle is independent from the ATP-dependent dissociation of kinesin II from microtubules, illustrating that our data reflect a novel mechanism for motor dissociation and are not a result of impaired microtubule association. According to our model, neither the assembly of the IFT particle nor the recruitment of kinesin II requires IFT57.

Knockdown of IFT20 has been shown to abolish cilia in cultured mammalian cells, indicating that IFT20 is essential for IFT. Our data indicate that IFT20 is not essential for IFT but does play a vital role in effective transport. The more severe phenotype described in cultured cells may reflect additional roles of IFT20 in post-Golgi to cilium trafficking of proteins. Consistent with this, Follit et al. (Follit et al., 2006) observe a reduction in the amount of polycystin 2 that is trafficked to the cilium when IFT20 is partially knocked down in cultured mammalian cells. As we show that loss of IFT57 abolishes the interaction between IFT20 and the IFT particle, we are able to separate the Golgi and ciliary functions of IFT20 and demonstrate its role within the IFT particle and that IFT20 is necessary only for efficient IFT.

In conclusion, we have provided novel details about IFT function in vertebrate photoreceptors that probably have broader implications for IFT function in a wide variety of tissues. First, we have demonstrated that IFT57 is not absolutely required for ciliogenesis and transport in photoreceptors but is required for ciliary elongation (e.g. outer segment growth) and the long-term maintenance of photoreceptor survival. Combined with previous results demonstrating that loss of IFT81 or IFT140 does not affect photoreceptor development, it is likely that most, but not all, IFT proteins are required for ciliogenesis in all vertebrate tissues, and the composition of the IFT particle varies from tissue to tissue. Second, we have provided evidence that presents novel insights into how IFT20 associates with the IFT particle, and the mechanism by which kinesin II dissociates from the IFT particle. These data illustrate how proper dissociation of kinesin II is necessary for efficient IFT and show the functional nature of two previously described interactions within the IFT particle. Additional biochemical studies are necessary to elucidate which IFT subunit(s) mediate the interaction of the particle with kinesin II, the mechanism by which the IFT particle assembles and the mechanisms that mediate kinesin II dissociation from the IFT particle. Finally, the structure and function of cilia varies with different tissues and the composition of the IFT particle may reflect this diversity. Identification of IFT genes required for photoreceptor development may help predict whether mutations in specific IFT genes will lead to retinal disease.

Materials and Methods

Zebrafish care and maintenance

The *oval* allele is an ENU-induced point mutation that caused a T-A transition, resulting in a premature stop codon in exon 11 and a null mutation in the *ift88* gene. The IFT88 mutant line was a gift from Jarema Malicki (Doerre and Malicki, 2002) and the *ift57* mutation has been previously described (Gross et al., 2005). Zebrafish were maintained according to standard procedures (Westerfield, 1995).

Morpholino knockdown

Morpholino knockdown of IFT57 was carried out using morpholinos directed against the splice site, sequence 5′-GTTATCGCCTCACCAGGGTTCGAAG-3′. A morpholino designed against the 5′UTR of IFT88, sequence 5′-TTATTAAACAGAAATACTCCCA-3′ was used to knock down IFT88 gene expression. Both morpholinos used have been described previously (Tsujikawa and Malicki, 2004) and were synthesized by Gene Tools.

Transient expression of IFT20-GFP

An IFT20-GFP fusion construct driven by the zebrafish opsin promoter was obtained from Dr Joe Besharse (Medical College of Wisconsin). Transgenic photoreceptors were generated as described (Perkins et al., 2002) and analyzed by immunohistochemistry as described below.

Histology: light microscopy and transmission electron microscopy (TEM)

Embryos were processed for light microscopy and TEM histology as previously described (Schmitt and Dowling, 1999). Histological sections were stained with a solution of 1% Azure Blue, 1% Methylene Blue and 1% sodium borate (Electron Microscopy Sciences). For immunogold labeling, staged embryos were fixed in 4% paraformaldehyde, 0.5% glutaraldehyde and 1% tannic acid in 0.1 M sodium cacodylate buffer (pH 7.4) overnight at 4° C. Embryos were washed in 0.15 M sodium cacodylate buffer at 4°C and dehydrated in a graded ethanol series with 1% pphenylenediamine. Specimens were embedded in LR-White resin (Electron Microscopy Sciences) and polymerized overnight at 55°C. For immunolocalization, incubations were carried out in a PELCO Biowave (Ted Pella) at low wattage, at 30°C. Grids were incubated in blocking solution (PBST + 4% cold water fish gelatin), then in primary antibody (1D1 1:50) diluted in blocking solution. Grids were washed with PBS then incubated in secondary antibody, donkey anti-mouse 18 nm colloidal gold (Jackson Immuno Research 1:30) diluted in TBST (TBST+2% normal donkey serum +4% coldwater fish gelatin). Grids were washed with TBS and then fixed with 1% glutaraldehyde and post stained with 2% uranyl acetate. Photographs were obtained on a JEOL 1200EX transmission electron microscope and images processed using Adobe Photoshop.

Antibody production

Rabbit polyclonal antibodies were generated against synthetic peptides corresponding to the C terminus of IFT88, IFT57, IFT52 and IFT20. The antigens were LEFADGELGDDLLPE, CMHATHLLEPNAQAY, CKKLNEEHDVDTAEARFSMY and CEAEQSEFIDQFILQK, respectively. The IFT88, IFT57 and IFT20 antibodies were generated and affinity purified by Bethyl Labs, while the IFT52 antibody was generated and affinity purified by Open Biosystems.

Immunohistochemistry

Immunohistochemistry was performed as previously described (Perkins et al., 2005). Images were obtained on an Olympus FV1000 confocal microscope or a Zeiss ImagerZ1 fluorescence microscope fitted with an ApoTome. Images were prepared using Adobe Photoshop software. The following list of primary antibodies were used, followed by the dilution used: 1D1 (1:200) (Fadool, 1999), cone opsin antibodies (1:200) (Vihtelic et al., 1999), ZPR1 (Zebrafish International Resource Center 1:200), anti-acetylated tubulin (Sigma 1:500), anti-syntaxin 6 (BD Bioscience 1:200) and anti-IFT88 (1:5000). The appropriate fluorescently conjugated antibodies (Jackson Immunological) were used at 1:500 dilution. Slides were counterstained with DAPI (Invitrogen) to label DNA.

Immunoprecipitation

Wild type and IFT57 mutants (4 dpf) were collected and homogenized using 200-250 larvae per reaction in IP lysis buffer (PBS + 1% Triton + 5 mM EDTA) supplemented with a cocktail of protease inhibitors (Complete-mini EDTA Free, Roche). Samples were lightly sonicated and lysates subsequently clarified by centrifugation at 16,100 ***g*** at 4°C for 15 minutes. Lysates were then precleared with ExactaCruz F preclearing matrix (Santa Cruz Biotechnology) according to manufacturer's instructions. Polyclonal rabbit anti-IFT88 antibody was bound to ExactaCruz F IP matrix per instructions. An equivalent amount of normal rabbit IGG (Santa Cruz Biologicals) was bound to ExactaCruz F IP matrix as a negative control. Lysates were then pooled and normalized for total protein concentration before incubation overnight at 4°C with antibody-IP matrix on a rocking platform. The IP matrix was pelleted by low speed centrifugation and washed twice with cold PBS and then five times with cold IP lysis buffer. Samples were eluted from IP matrix by boiling 5 minutes in 45 μl of 2× Laemmli buffer and then 20 μl loaded on an SDS-PAGE gel for analysis. For ATP experiments, prior to addition

of antibody-IP matrix to the lysates, ATP (Roche) was added to achieve either 1 or 10 mM final concentration. The lysates were incubated with ATP at 4°C for 1 hour prior to the addition of antibody-IP matrix to the lysates.

SDS-PAGE and immunoblot analysis

Heads of 4 dpf zebrafish were homogenized in IP lysis buffer at a volume of 3 μl per head, then lightly sonicated. SDS sample buffer (4×) was added to the lysate and the samples were then boiled for 5 minutes. prior to centrifugation at 16,100 ***g*** for 10 minutes and subsequent loading on a 10% PAGE gel. Following electrophoresis, proteins were blotted onto PVDF membranes (BioRad) and subjected to immunodetection using standard protocols. The following dilutions of primary antibodies were used: K2.4 (mouse anti-KIF3A, Covance 1:10,000), rabbit anti-IFT88 (1:5000), rabbit anti-IFT52 (1:5000), rabbit anti-IFT20 (1:5000), rabbit anti IFT57 (1:5000) and mouse anti-acetylated tubulin (Sigma, 1:10,000).

Acknowledgements

The authors thank Jarema Malicki for providing the *oval*^{tz288b} (IFT88) mutant line, Joseph Besharse for providing the xops:IFT20-GFP plasmid, and Tom Vihtelic for providing the cone opsin antibodies. The authors are indebted to Ann Ellis in the Texas A&M Microscopy Imaging Center for assistance with transmission electron microscopy. This work was supported by the NIH grant RO1EY017037 to B.D.P.

References

Amsterdam A, Hopkins N. Retrovirus-mediated insertional mutagenesis in zebrafish. Methods Cell Biol 1999;60:87–98. [PubMed: 9891332]

Baker SA, Freeman K, Luby-Phelps K, Pazour GJ, Besharse JC. IFT20 links kinesin II with a mammalian intraflagellar transport complex that is conserved in motile flagella and sensory cilia. J. Biol. Chem 2003;278:34211–34218. [PubMed: 12821668]

Beales PL, Bland E, Tobin JL, Bacchelli C, Tuysuz B, Hill J, Rix S, Pearson CG, Kai M, Hartley J, et al. IFT80, which encodes a conserved intraflagellar transport protein, is mutated in Jeune asphyxiating thoracic dystrophy. Nat. Genet 2007;39:727–729. [PubMed: 17468754]

Berson EL, Rosner B, Sandberg MA, Weigel-DiFranco C, Dryja TP. Ocular findings in patients with autosomal dominant retinitis pigmentosa and rhodopsin, proline-347-leucine. Am. J. Ophthalmol 1991;111:614–623. [PubMed: 2021172]

Besharse, JC.; Horst, CJ. The Photoreceptor Connecting Cilium. A Model for the Transition Zone. Plenum; New York: 1990.

Bisgrove BW, Snarr BS, Emrazian A, Yost HJ. Polaris and Polycystin-2 in dorsal forerunner cells and Kupffer's vesicle are required for specification of the zebrafish left-right axis. Dev. Biol 2005;287:274–288. [PubMed: 16216239]

Cole DG. Kinesin-II, coming and going. J. Cell Biol 1999;147:463–466. [PubMed: 10545491]

Cole DG. The intraflagellar transport machinery of Chlamydomonas reinhardtii. Traffic 2003;4:435–442. [PubMed: 12795688]

Cole DG, Diener DR, Himelblau AL, Beech PL, Fuster JC, Rosenbaum JL. Chlamydomonas kinesin-II-dependent intraflagellar transport (IFT): IFT particles contain proteins required for ciliary assembly in Caenorhabditis elegans sensory neurons. J. Cell Biol 1998;141:993–1008. [PubMed: 9585417]

De Robertis E. Some observations on the ultrastructure and morphogenesis of photoreceptors. J. Gen. Physiol 1960;43(Suppl):1–13. [PubMed: 13814989]

Doerre G, Malicki J. Genetic analysis of photoreceptor cell development in the zebrafish retina. Mech. Dev 2002;110:125–138. [PubMed: 11744374]

Fadool JM, Fadool DA, Moore JC, Linser PJ. Characterization of monoclonal antibodies against zebrafish retina. Invest. Opthamol. Vis. Sci. Suppl 1999;40:1251.

Follit JA, Tuft RA, Fogarty KE, Pazour GJ. The intraflagellar transport protein IFT20 is associated with the Golgi complex and is required for cilia assembly. Mol. Biol. Cell 2006;17:3781–3792. [PubMed: 16775004]

Green ES, Menz MD, LaVail MM, Flannery JG. Characterization of rhodopsin mis-sorting and constitutive activation in a transgenic rat model of retinitis pigmentosa. Invest. Ophthalmol. Vis. Sci 2000;41:1546–1553. [PubMed: 10798675]

Gross JM, Perkins BD, Amsterdam A, Egana A, Darland T, Matsui JI, Sciascia S, Hopkins N, Dowling JE. Identification of zebrafish insertional mutants with defects in visual system development and function. Genetics 2005;170:245–261. [PubMed: 15716491]

Han YG, Kwok BH, Kernan MJ. Intraflagellar transport is required in Drosophila to differentiate sensory cilia but not sperm. Curr. Biol 2003;13:1679–1686. [PubMed: 14521833]

Haycraft CJ, Swoboda P, Taulman PD, Thomas JH, Yoder BK. The C. elegans homolog of the murine cystic kidney disease gene Tg737 functions in a ciliogenic pathway and is disrupted in osm-5 mutant worms. Development 2001;128:1493–1505. [PubMed: 11290289]

Haycraft CJ, Schafer JC, Zhang Q, Taulman PD, Yoder BK. Identification of CHE-13, a novel intraflagellar transport protein required for cilia formation. Exp. Cell Res 2003;284:251–263. [PubMed: 12651157]

Hou Y, Qin H, Follit JA, Pazour GJ, Rosenbaum JL, Witman GB. Functional analysis of an individual IFT protein: IFT46 is required for transport of outer dynein arms into flagella. J. Cell Biol 2007;176:653–665. [PubMed: 17312020]

Houde C, Dickinson RJ, Houtzager VM, Cullum R, Montpetit R, Metzler M, Simpson EM, Roy S, Hayden MR, Hoodless PA, et al. Hippi is essential for node cilia assembly and Sonic hedgehog signaling. Dev. Biol 2006;300:523–533. [PubMed: 17027958]

Huangfu D, Liu A, Rakeman AS, Murcia NS, Niswander L, Anderson KV. Hedgehog signalling in the mouse requires intraflagellar transport proteins. Nature 2003;426:83–87. [PubMed: 14603322]

Humphries MM, Rancourt D, Farrar GJ, Kenna P, Hazel M, Bush RA, Sieving PA, Sheils DM, McNally N, Creighton P, et al. Retinopathy induced in mice by targeted disruption of the Rhodopsin gene. Nat. Genet 1997;15:216–219. [PubMed: 9020854]

Kramer-Zucker AG, Olale F, Haycraft CJ, Yoder BK, Schier AF, Drummond IA. Cilia-driven fluid flow in the zebrafish pronephros, brain and Kupffer's vesicle is required for normal organogenesis. Development 2005;132:1907–1921. [PubMed: 15790966]

Lem J, Krasnoperova NV, Calvert PD, Kosaras B, Cameron DA, Nicolo M, Makino CL, Sidman RL. Morphological, physiological, and biochemical changes in rhodopsin knockout mice. Proc. Natl. Acad. Sci. USA 1999;96:736–741. [PubMed: 9892703]

Li T, Snyder WK, Olsson JE, Dryja TP. Transgenic mice carrying the dominant rhodopsin mutation P347S: evidence for defective vectorial transport of rhodopsin to the outer segments. Proc. Natl. Acad. Sci. USA 1996;93:14176–14181. [PubMed: 8943080]

Liu A, Wang B, Niswander LA. Mouse intraflagellar transport proteins regulate both the activator and repressor functions of Gli transcription factors. Development 2005;132:3103–3111. [PubMed: 15930098]

Lucker BF, Behal RH, Qin H, Siron LC, Taggart WD, Rosenbaum JL, Cole DG. Characterization of the intraflagellar transport complex B core: direct interaction of the IFT81 and IFT74/72 subunits. J. Biol. Chem 2005;280:27688–27696. [PubMed: 15955805]

Marszalek JR, Liu X, Roberts EA, Chui D, Marth JD, Williams DS, Goldstein LS. Genetic evidence for selective transport of opsin and arrestin by kinesin-II in mammalian photoreceptors. Cell 2000;102:175–187. [PubMed: 10943838]

Moritz OL, Tam BM, Hurd LL, Peranen J, Deretic D, Papermaster DS. Mutant rab8 impairs docking and fusion of rhodopsin-bearing post-golgi membranes and causes cell death of transgenic xenopus rods. Mol. Biol. Cell 2001;12:2341–2351. [PubMed: 11514620]

Murcia NS, Richards WG, Yoder BK, Mucenski ML, Dunlap JR, Woychik RP. The Oak Ridge Polycystic Kidney (orpk) disease gene is required for left-right axis determination. Development 2000;127:2347–2355. [PubMed: 10804177]

Nathans J. Rhodopsin: structure, function, and genetics. Biochemistry 1992;31:4923–4931. [PubMed: 1599916]

Orozco JT, Wedaman KP, Signor D, Brown H, Rose L, Scholey JM. Movement of motor and cargo along cilia. Nature 1999;398:674. [PubMed: 10227290]

Ou G, Blacque OE, Snow JJ, Leroux MR, Scholey JM. Functional coordination of intraflagellar transport motors. Nature 2005;436:583–587. [PubMed: 16049494]

Pazour GJ, Rosenbaum JL. Intraflagellar transport and cilia-dependent diseases. Trends Cell Biol 2002;12:551–555. [PubMed: 12495842]

Pazour GJ, Dickert BL, Vucica Y, Seeley ES, Rosenbaum JL, Witman GB, Cole DG. Chlamydomonas IFT88 and its mouse homologue, polycystic kidney disease gene tg737, are required for assembly of cilia and flagella. J. Cell Biol 2000;151:709–718. [PubMed: 11062270]

Pazour GJ, Baker SA, Deane JA, Cole DG, Dickert BL, Rosenbaum JL, Witman GB, Besharse JC. The intraflagellar transport protein, IFT88, is essential for vertebrate photoreceptor assembly and maintenance. J. Cell Biol 2002;157:103–113. [PubMed: 11916979]

Pedersen LB, Miller MS, Geimer S, Leitch JM, Rosenbaum JL, Cole DG. Chlamydomonas IFT172 is encoded by FLA11, interacts with CrEB1, and regulates IFT at the flagellar tip. Curr. Biol 2005;15:262–266. [PubMed: 15694311]

Perkins BD, Kainz PM, O'Malley DM, Dowling JE. Transgenic expression of a GFP-rhodopsin COOH-terminal fusion protein in zebrafish rod photoreceptors. Vis. Neurosci 2002;19:257–264. [PubMed: 12392175]

Perkins BD, Nicholas CS, Baye LM, Link BA, Dowling JE. dazed gene is necessary for late cell type development and retinal cell maintenance in the zebrafish retina. Dev. Dyn 2005;233:680–694. [PubMed: 15844196]

Postlethwait JH, Woods IG, Ngo-Hazelett P, Yan YL, Kelly PD, Chu F, Huang H, Hill-Force A, Talbot WS. Zebrafish comparative genomics and the origins of vertebrate chromosomes. Genome Res 2000;10:1890–1902. [PubMed: 11116085]

Qin H, Rosenbaum JL, Barr MM. An autosomal recessive polycystic kidney disease gene homolog is involved in intraflagellar transport in C. elegans ciliated sensory neurons. Curr. Biol 2001;11:457–461. [PubMed: 11301258]

Qin H, Wang Z, Diener D, Rosenbaum J. Intraflagellar transport protein 27 is a small G protein involved in cell-cycle control. Curr. Biol 2007;17:193–202. [PubMed: 17276912]

Rosenbaum JL, Witman GB. Intraflagellar transport. Nat. Rev. Mol. Cell Biol 2002;3:813–825. [PubMed: 12415299]

Schmitt EA, Dowling JE. Early retinal development in the zebrafish, Danio rerio: light and electron microscopic analyses. J. Comp. Neurol 1999;404:515–536. [PubMed: 9987995]

Snell WJ, Pan J, Wang Q. Cilia and flagella revealed: from flagellar assembly in Chlamydomonas to human obesity disorders. Cell 2004;117:693–697. [PubMed: 15186771]

Snow JJ, Ou G, Gunnarson AL, Walker MR, Zhou HM, Brust-Mascher I, Scholey JM. Two anterograde intraflagellar transport motors cooperate to build sensory cilia on C. elegans neurons. Nat. Cell Biol 2004;6:1109–1113. [PubMed: 15489852]

Sun Z, Amsterdam A, Pazour GJ, Cole DG, Miller MS, Hopkins N. A genetic screen in zebrafish identifies cilia genes as a principal cause of cystic kidney. Development 2004;131:4085–4093. [PubMed: 15269167]

Sung CH, Makino C, Baylor D, Nathans J. A rhodopsin gene mutation responsible for autosomal dominant retinitis pigmentosa results in a protein that is defective in localization to the photoreceptor outer segment. J. Neurosci 1994;14:5818–5833. [PubMed: 7523628]

Tai AW, Chuang JZ, Bode C, Wolfrum U, Sung CH. Rhodopsin's carboxy-terminal cytoplasmic tail acts as a membrane receptor for cytoplasmic dynein by binding to the dynein light chain Tctex-1. Cell 1999;97:877–887. [PubMed: 10399916]

Tam BM, Moritz OL, Hurd LB, Papermaster DS. Identification of an outer segment targeting signal in the COOH terminus of rhodopsin using transgenic Xenopus laevis. J. Cell Biol 2000;151:1369–1380. [PubMed: 11134067]

Tsujikawa M, Malicki J. Intraflagellar transport genes are essential for differentiation and survival of vertebrate sensory neurons. Neuron 2004;42:703–716. [PubMed: 15182712]

Vihtelic TS, Doro CJ, Hyde DR. Cloning and characterization of six zebrafish photoreceptor opsin cDNAs and immunolocalization of their corresponding proteins. Vis. Neurosci 1999;16:571–585. [PubMed: 10349976]

Westerfield, M. The Zebrafish Book. University of Oregon Press; Eugene, OR: 1995.

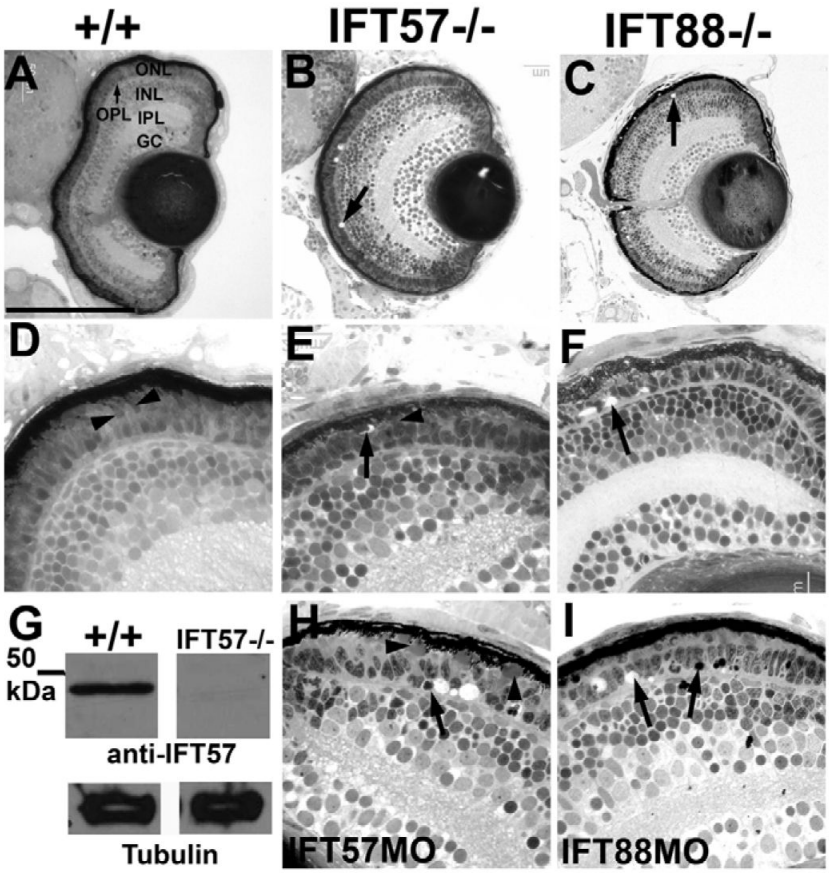

Fig. 1.

Histological sections of 4 dpf wild-type, IFT57 and IFT88 mutant and morphant retinas. (A) Wild-type retinas at 4 dpf are fully laminated, and the outer nuclear layer (ONL), inner nuclear layer (INL) and retinal ganglion cells (RGC) are present. The outer plexiform layer (OPL) and the inner plexiform layer (IPL) are easily observable. (B,C) Lamination and cellular differentiation are unaffected in both IFT57 and IFT88 mutants; however, acellular holes (arrows) in the ONL are observed. (D) High-magnification images of wild-type retinas showing photoreceptor outer segments (arrowheads). Outer segments are not observed in IFT88 mutants (C); however, short outer segments are observed in IFT57 mutants (arrowhead). (G) Western blot analysis of IFT57 mutants at 4 dpf. No IFT57 protein is observed in IFT57 mutants (upper blot, lane 2). Blots probed with anti-acetylated tubulin serve as a loading control (lower blot). (H,I) Histological analysis of IFT57 and IFT88 morphants phenocopy the IFT57 and IFT88 mutations, respectively. Arrowheads in D,E,H indicate outer segments and arrows in E,H,I indicate acellular holes or pyknotic nuclei. Scale bar: 100 μm in A-C; 20 μm in D-F,H,I.

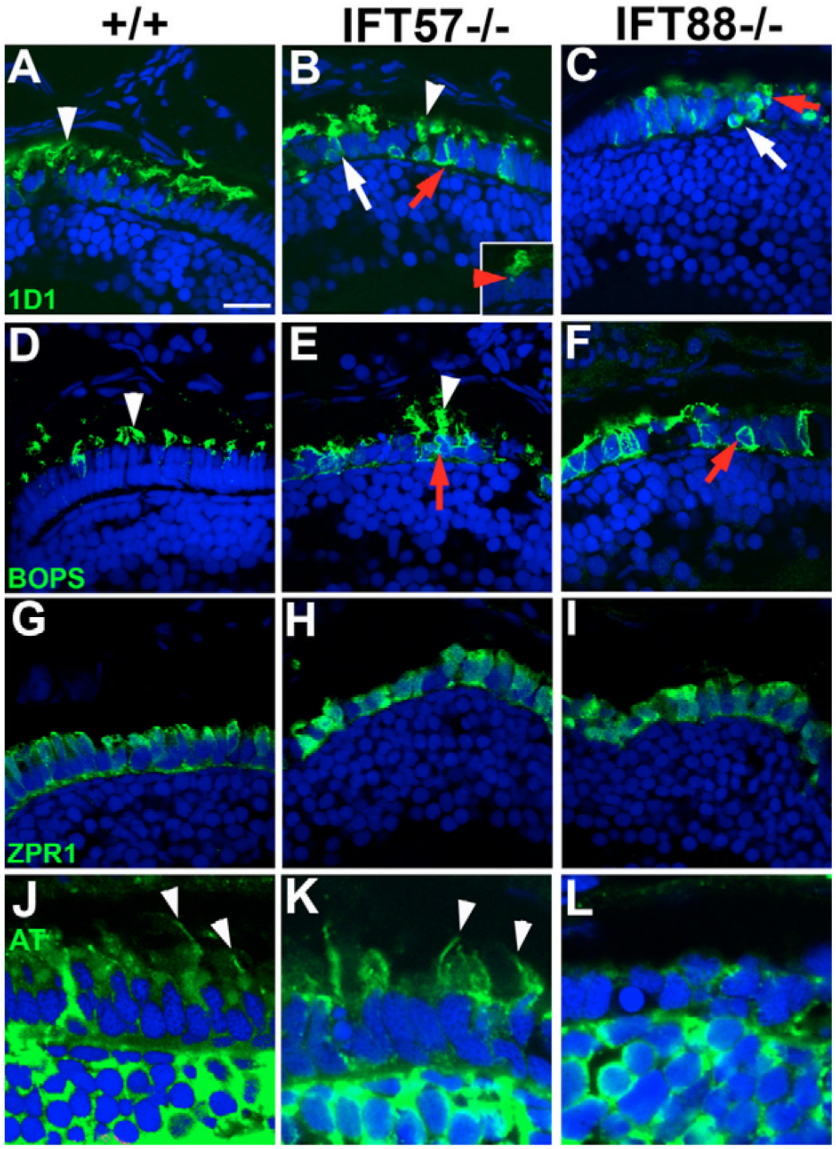

Fig. 2.

Immunohistochemical analysis of wild type and IFT mutants. Retinal cryosections of 4 dpf larvae were stained with 1D1, an antibody that labels rhodopsin, with BOPS, an antibody against blue cone opsin, and with ZPR1, an antibody that recognizes an unknown epitope of red-green double cones. In addition, anti-acetylated tubulin (AT) was used to label microtubules and visualize cilia. In all panels, immunolabel is shown in green and nuclei are counterstained with DAPI (blue). (A) Wild-type photoreceptors have rhodopsin localized almost exclusively to the outer segment (arrowhead). (B) IFT57 mutants display significant rhodopsin localization to the outer segment (arrowhead), but punctate areas of rhodopsin mislocalization (inset, red arrowhead) are observed, as well as mislocalization of rhodopsin through the plasma membrane (red arrow). (C) IFT88 mutant photoreceptors have rhodopsin completely mislocalized throughout the plasma membrane (red arrow) and both IFT mutants exhibit cell death in the photoreceptor layer, as indicated by condensed and bright DAPI-labeled nuclei of pyknotic cells (white arrow). (D-F) Blue opsin also localizes to the outer segments of blue cones. IFT57 and IFT88 mutants exhibit a similar pattern of mislocalization with blue cone opsin as seen with rhodopsin. (G-I) ZPR1 labeling indicates red-green double-

cone morphology at 4 dpf in wild type. IFT57 and IFT88 mutants have shorter cones when measured in the apical-basal axis, and adopt an abnormal morphology. (J-L) Anti-acetylated tubulin stains microtubules in the connecting cilia (arrowheads) that project apically from the cell body in both wild type and IFT57 mutants, but not in IFT88 mutants. Scale bar: 10 μm.

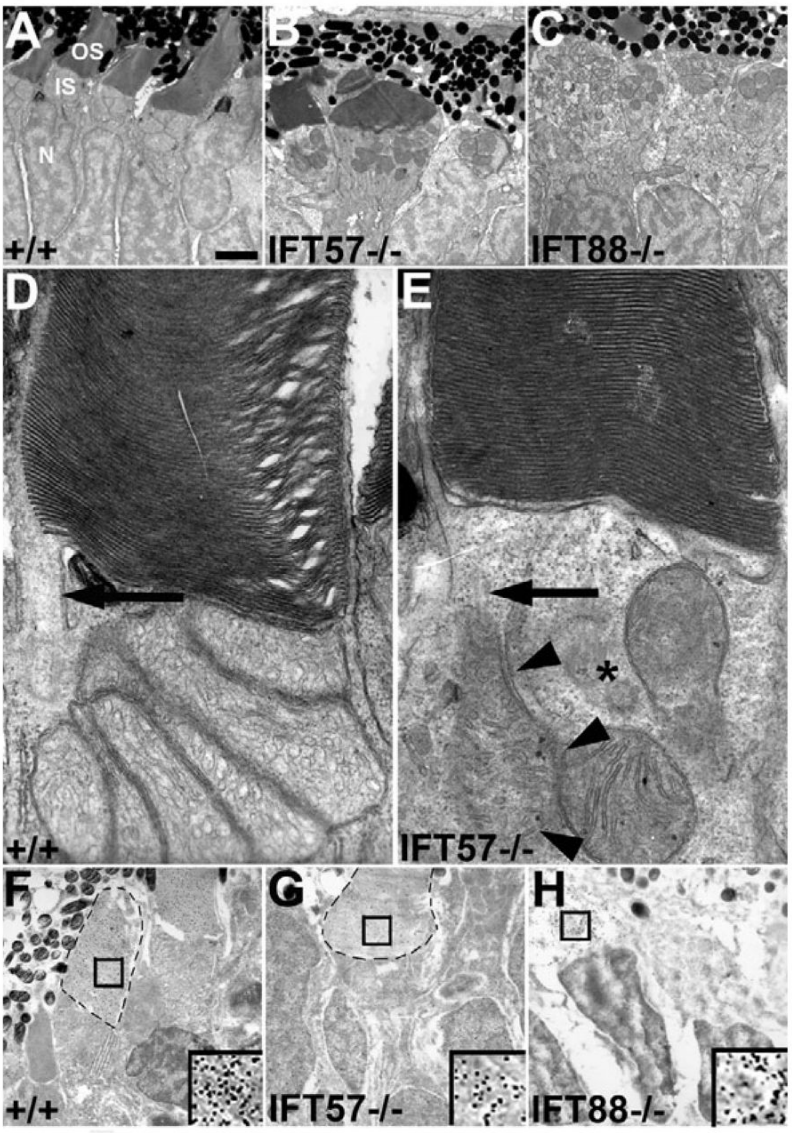

Fig. 3.

Transmission electron microscopy of 4 dpf wild-type, IFT57 and IFT88 mutant retinas. (A-C) Low-magnification electron micrographs of wild-type and mutant retinas, illustrating the outer segment (OS), inner segment (IS) and nucleus (N). Wild type and IFT57 mutants both exhibit photoreceptor outer segments, but IFT88 mutants lack these structures. (D,E) High-magnification micrographs of wild-type and IFT57 mutant retinas. Wild-type photoreceptors exhibit well-organized disk stacking within the outer segment, and the connecting cilium (black arrow) is observable. IFT57 mutants also demonstrate normal disk stacking within the outer segment, and the base of the connecting cilium (black arrow) is evident. An accumulation of vesicles (black arrowheads) is observed at the base of the cilium. Asterisk indicates centrioles oriented at right angles within the photoreceptor. (F-H) Immunogold labeling of rhodopsin in wild-type retinas shows dense labeling within the outer segment. Outer segments are outlined by broken lines and insets are magnified views of the boxed area in each panel, which illustrate gold particle density. IFT57 mutant outer segments demonstrate a lower density of label when compared with wild type, whereas rhodopsin localizes most densely to the apical part of the

photoreceptor in IFT88 mutants. Scale bar: 2 μm in A-C; 200 nm in D,E; 0.75 μm in F; 1 μm in G,H.

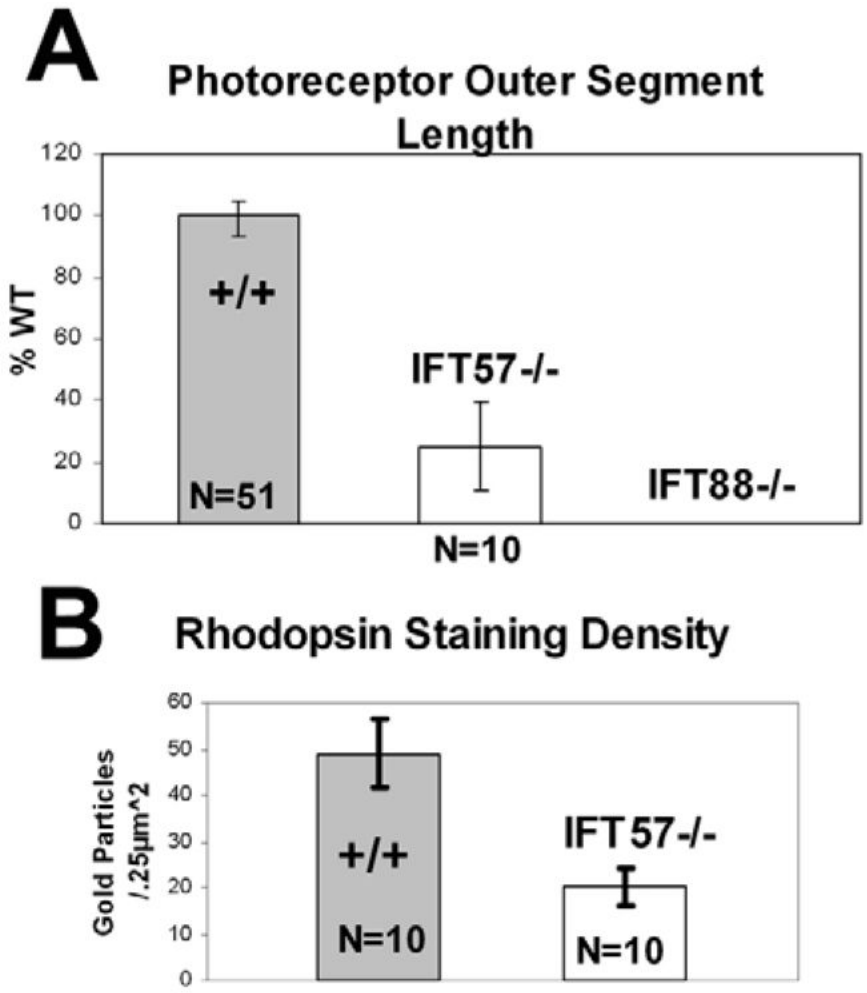

Fig. 4.

Quantification of photoreceptor outer segment length and rhodopsin staining density within the outer segment in wild type and IFT57 mutants. (A) IFT57 mutant photoreceptor outer segments are reduced in length by 75% when compared with age-matched wild-type photoreceptors. Data were taken from retinas of four animals for both wild type and IFT mutants. (B) Photoreceptor outer segments in IFT57 mutants contain 59% less rhodopsin. Staining density was determined by counting colloidal gold particles in a random 0.25 μm^2 region of rod outer segments with each data point obtained from a unique outer segment. Data were obtained from retinas of four animals for both wild type and IFT57 mutants. (A) $P<0.01$, (B) $P<0.0001$, as determined by a Student's *t*-test.

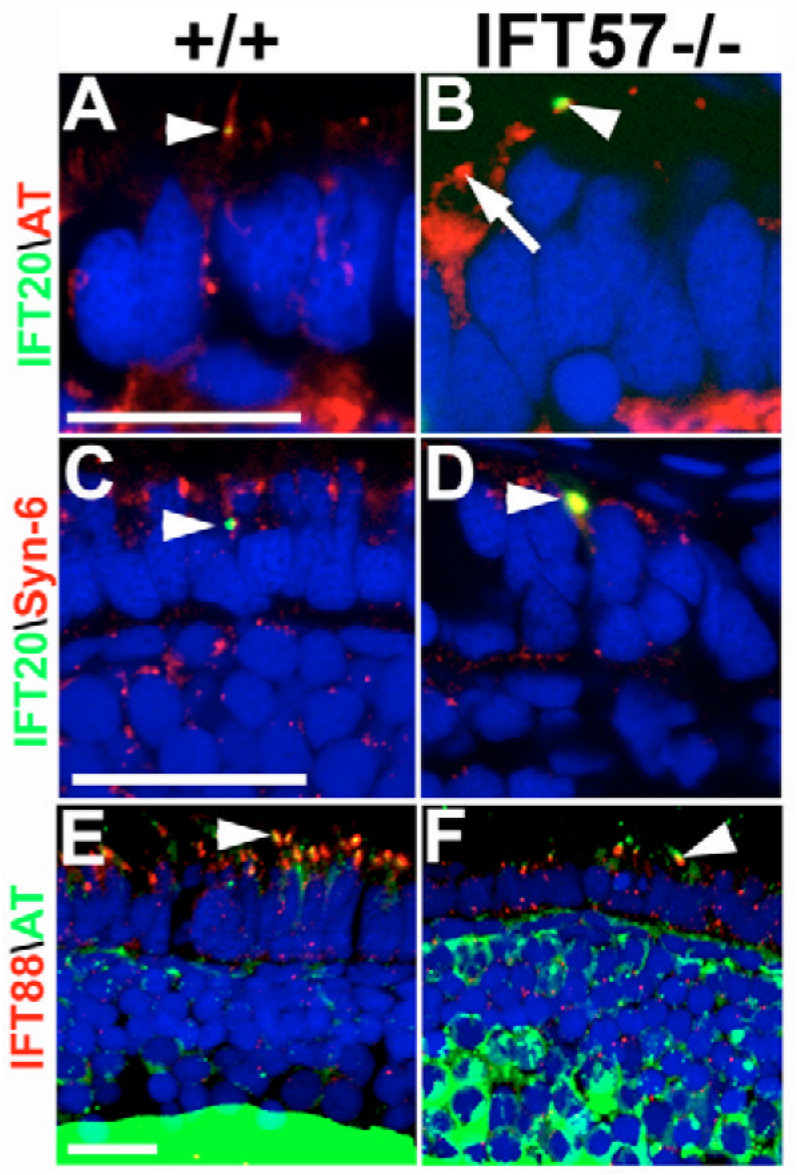

Fig. 5.

IFT20 and IFT88 localize to the base of the cilium in IFT57 mutant rods. (A) Wild-type rods expressing an IFT20-GFP transgene exhibit IFT20 localization at the base of the cilium (acetylated tubulin), where it colocalizes with acetylated tubulin (yellow; arrowhead). As the embryos do not carry an integrated transgene, only a small number of rod photoreceptors in the retina exhibit expression. (B) Loss of IFT57 does not affect IFT20-GFP localization to connecting cilia (arrowhead). Arrow indicates the connecting cilia in a neighboring cell that does not express the IFT20-GFP transgene. (C,D) In the presence or absence of IFT57, IFT20-GFP localized to the Golgi apparatus, where it colocalizes with syntaxin 6 (arrowhead). (E) IFT88 localizes to the base of the connecting cilium (arrowhead) in wild-type photoreceptors as well as in (F) IFT57 mutant photoreceptors. Abbreviations: AT, acetylated tubulin; Syn-6, syntaxin 6. Scale bar: 10 μm in A,B,E,F; 40 μm in C,D.

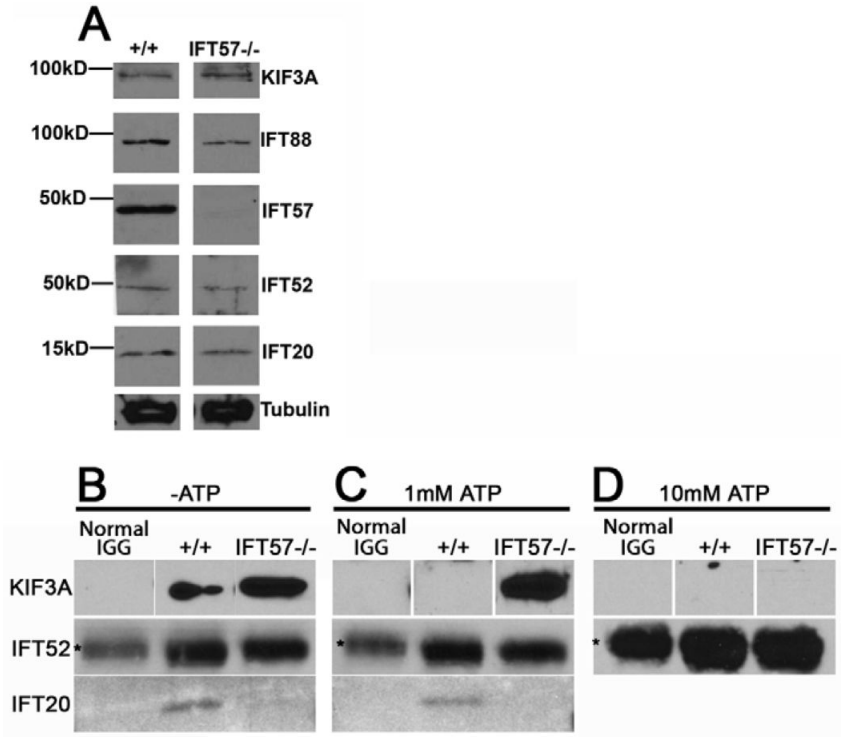

Fig. 6.

Biochemical analysis of IFT57 mutants. (A) Western blot of lysates generated from the larval heads of 4 dpf wild type and IFT57 mutants. Mutation of IFT57 does not significantly alter the abundance of any other IFT protein other than IFT57. (B) Lysates of wild type (+/+) or IFT57 mutants (IFT57−/−) were incubated with rabbit antibodies against zebrafish IFT88 or normal rabbit IGG as a negative control. Immunoprecipitates were subsequently blotted with antibodies against KIF3A, IFT52 and IFT20. In IFT57 mutants, IFT20 is not precipitated along with the IFT complex, whereas more KIF3A is precipitated. (C) The addition of 1 mM ATP to lysates blocks the association of KIF3A with the IFT particle in wild-type lysates but not in IFT57 lysates. Lysates were prepared as described above, and then ATP was added to a final concentration of 1 mM prior to the addition of IFT88 antibody and precipitation. (D) The addition of 10 mM ATP blocks the association of KIF3A with the IFT particle in both wild-type and mutant lysates. Asterisks indicate IGG heavy chain band from precipitating antibody on immunoblots.

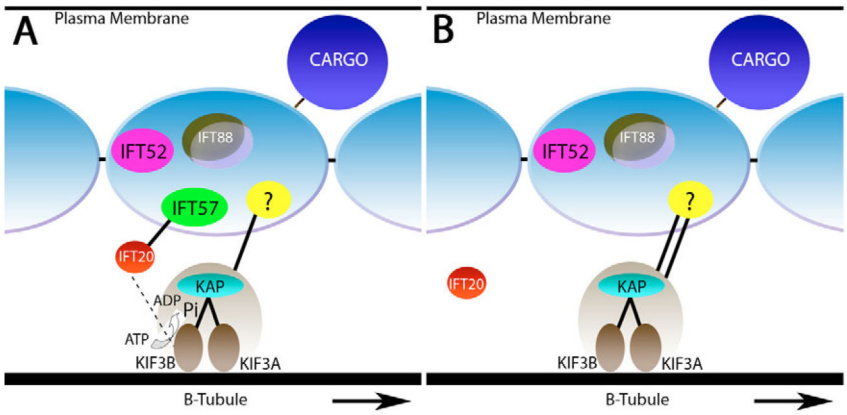

Fig. 7.

IFT57 and IFT20 mediate the ATP-dependent dissociation of kinesin. (A) A model describing the nature of protein interactions within the IFT complex. IFT57 tethers IFT20 to the IFT particle, while kinesin binds to the IFT particle through an unknown entity. IFT20 physically interacts with KIF3B and mediates the ATP-dependent dissociation of kinesin. (B) In the absence of IFT57, IFT20 can no longer associate with the IFT particle. However, the interaction of kinesin with the IFT particle is stabilized by loss of IFT57 and IFT20 from the IFT particle.